ELSEVIER

Atmospheric Environment 38 (2004) 5887–5894

ATMOSPHERIC ENVIRONMENT

www.elsevier.com/locate/atmosenv

Optical coherency of sunphotometry, sky radiometry and lidar measurements during the early phase of Pacific 2001

N.T. O'Neill[a,*], K.B. Strawbridge[b], S. Thulasiraman[a], J. Zhang[a], A. Royer[a], J. Freemantle[a]

[a] *CARTEL, Université de Sherbrooke, Sherbrooke, Qué., Canada, J1K 2R1*

[b] *Meteorological Service of Canada, Air Quality Processes Research Division, Centre For Atmospheric Research Experiments, 6248 Eighth Line, R.R. #1, Egbert, Ont., Canada, L0L 1N0*

Received 1 August 2003; received in revised form 10 December 2003; accepted 22 December 2003

Abstract

Passive sunphotometry and sky radiometry data at sites in the Lower Fraser Valley (Langley-Lochiel) and Saturna Island were synchronously acquired with ground-based scanning lidar (Rapid Acquisition Scanning Aerosol Lidar, RASCAL) and airborne lidar (AERosol Imaging Airborne Lidar, AERIAL) during the Pacific 2001 Air Quality Study. The temporal and spatial behavior of these optical measurements is investigated during a pollution event which occurred from 13 to 16 August 2001. A mid-day minimum in lidar-derived extinction to backscatter ratios (S_a) values, was attributed, at least in part, to the relative humidity (RH) induced optical influence of the column integrated fine mode and/or coarse mode particles in the PBL. Systematically larger S_a values predicted by the sunphotometer and sky radiance inversions were hypothesized to be due to differences between the retrieved refractive index and the actual refractive index of the coarse mode. Aerosol optical depth differences were within maximum error bounds (0.02) when comparing the sunphotometry with spatial maps derived from AERIAL transects. Daily temporal trends of optical and microphysical parameters derived from sunphotometry and sky radiance data at this site were consistent with information deduced from the lidar and meteorological data; while the daily aerosol optical depth decrease was clearly associated with particle removal induced by daytime sea-breeze advection, a significant-to-dominant part of this decrease was associated with decreasing RH growth effects on at least one day.

Keywords: Aerosol optical depth; Air quality; Pacific2001; Lidar; Sun photometry

1. Introduction

The relationship between aerosol vertical profile information and the variability of passively derived optical parameters (the aerosol optical depth or AOD in particular) is an open research question and a key motivation for recent large-scale aerosol characterization experiments such as ACE-1, TARFOX, ACE-2 and INDOEX (see for example Ferrare et al., 2000; Ansmann et al., 2002; Pelon et al., 2002). Lidar and passive optical measurements carried out over the duration of such experiments can serve as a means of investigating this relationship. Such measurements are interesting in their own right as a means of

*Corresponding author.

E-mail addresses: norm.oneill@usherbrooke.ca (N.T. O'Neill), kevin.strawbridge@ec.gc.ca (K.B. Strawbridge).

1352-2310/$ - see front matter
doi:10.1016/j.atmosenv.2003.12.049

understanding the influence of local atmospheric inhomogenieties (vertical and horizontal) on the retrieval of passively measured optical parameters but as well in terms of inferring certain optical parameters (such as the extinction-to-backscatter ratio) from the combination of both types of data.

In order to appreciate the variation of optical parameters derived from passive sunphotometry or passive sky radiometry one must, in principle, understand the influence of aerosol particle size, number density and particle type as a function of altitude. Ground-based Rayleigh/Mie lidar measurements provide vertical profiles of essentially the backscattering coefficient (the product of the size and type dependent scattering phase function and the predominantly number density dependent volume scattering coefficient) while sunphotometry and sky scanning radiometry provide information on the vertically integrated volume scattering coefficient and the vertically averaged phase function and single scattering albedo. If the lidar system can be scanned in elevation and azimuth then (2D) azimuthal sky sections of the volume backscatter yield a detailed picture of the local atmosphere which can be used to interpret the temporal variation of the optical parameters derived from the passive radiometry. The line-of-sight integration of lidar backscatter yields optical averages of the backscattering coefficient which can be directly linked to the passive optical parameters and hence can be used to infer the reasons for perturbations of the passive parameters from the values expected for a horizontally homogeneous atmosphere.

Multi-flight-line airborne lidar provides a 3D matrix of backscatter coefficient which can be resampled to a geographical grid to yield a regional scale (roughly static) picture of aerosol optics. This information, combined with temporal sunphotometry at two or more stations yields a spatio-temporal sampling of aerosol optical properties which can greatly assist the interpretation of the optical mechanisms prevalent during a given event.

Airborne lidar, ground-based scanning lidar and passive sun and sky radiometry techniques were synchronously employed as indicators of aerosol behavior during the Pacific 2001 Air Quality Study. This study consisted of a comprehensive suite of meteorological, microphysical, chemical and optical measurements carried out within the Lower Fraser Valley (LFV) over the latter part of August 2001 (Li, 2004). The LFV is of interest because its complex and turbulent flow patterns are coupled with the polluting influence of a larger urban center (Vancouver, BC).

Snyder and Strawbridge (2004) point out that the Pacific 2001 measurement period was broken up into four meteorological phases; the stagnant phase from 13 to 16 August, the well-mixed phase from 16 to 20 August, the major trough phase from 25 to 28 August and the minor trough phase from 29 August to 01 September. In this paper we focus on the stagnant phase since this period of time was characterized by conditions which were largely cloudless but of highly variable optical (aerosol) turbidity.

2. Methodology

Ground-based scanning lidar (RASCAL—Rapid Acquisition SCanning Aerosol Lidar) measurements were carried out on most non-precipitating days from 14 to 31 August at Lochiel School in Langley (49° 01′ N., 122° 36′ W), a suburban to rural transition site southeast of Vancouver (Strawbridge and Snyder, 2004a). Elevation scans at roughly 0, 85 and 306 azimuthal degrees from true north were performed 16 h per day (approximately 3 min per elevation scan) to yield 2D sky cross sections of backscatter ratio (unitless ratio of aerosol to Rayleigh backscatter coefficient). A CIMEL sunphotometer/sky radiometer belonging to the AERONET network was placed alongside the RASCAL system while a second CIMEL belonging to the AEROCAN network (a Canadian subnet of AERONET) was operated on Saturna Island, about 50 km southwest of the Lochiel site in the Strait of Georgia (48° 46′ N., 123° 07′ W). An airborne lidar system (AERIAL—AERosol Imaging Airborne Lidar) was flown on 14, 15, 20, 25, 26 and 29 August along north–south flight lines which spanned the area between Lochiel School and Saturna Island (Strawbridge and Snyder, 2004b). Both the AERIAL and RASCAL lidar systems operate at a wavelength of 1064 nm while the CIMEL sunphotometers acquire aerosol optical data in 7 spectral bands (340, 380, 440, 500, 670, 870, 1020 nm).

The integration of line-of-sight lidar profiles accompanied by assumptions of atmospheric homogeneity yield an output which is a function of the vertically averaged extinction-to-backscatter ratio (S_a) and the AOD (a definition of S_a can be found, for example, in Anderson et al., 2000). This permits one to estimate S_a by forcing the lidar derived AOD equal to sunphotometer values (as we did in the case of RASCAL) or of estimating the AOD variation assuming constant values of vertically averaged S_a (as we did in the case of AERIAL).

The sunphotometer extinction data were processed approximately every 15 min according to AERONET protocols (Holben et al., 1998) and were cloud screened and quality assured to the level 2.0 product (Smirnov et al., 2000). Separation of the total AOD at 500 nm into fine and coarse mode optical depths and the total Angstrom exponent into the fine mode Angstrom exponent was performed as defined in O'Neill et al. (2003). Inversion of the combined extinction and sky radiance data (acquired approximately once per hour)

yielded estimates of column integrated particle size distribution, refractive index and scattering phase function (Dubovik and King, 2000). The values of scattering phase function retrievals at 180° ($p(\pi)$) and single scattering albedo (ω_0) yielded vertically averaged S_a values ($1/\{\omega_0\, p(\pi)/(4\pi)\}$) which could be compared to the S_a values derived from the RASCAL data (i.e. where the computed lidar AODs are forced to be equal to the sunphotometer AODs).

It is noted that the 670 and 1020 nm channels of the Saturna Island CIMEL showed anomolous inter-band behavior which had a deleterious effect on spectral computations such as the Angstrom exponent and by extension on inferred quantities such as the particle size distribution. We accordingly restricted the use of this instrument to that of a tool for monitoring single band variations in AOD.

3. Spatial and temporal correlations at the regional scale

In their Pacific 2001 meteorological analysis, Snyder and Strawbridge (2004) indicate that a "stagnant" phase characterized by a daily pattern of regionally trapped pollution being gradually pushed into the LFV by sea breezes was the dominant mechanism from about 13 to 16 August. During the night this pollution would be typically vented back out into the mouth of the LFV and the Georgia Strait thus creating conditions for a more regional pollution haze the following morning. Consistent with this analysis one can observe (Fig. 1) a recurring pattern of a daily AOD decrease from a morning maximum superimposed on a low frequency (multi-day) AOD variation extending across the nominal stagnant period. The Saturna Island site in the Georgia strait appears to share many of these same features except in the latter part of the stagnant period when the AOD is smaller and more stable.

Figs. 2a and b show continuous AOD maps generated from a resampling of north–south flight lines of AERIAL data acquired on 14 and 15 August, respectively. The S_a values used in computing AERIAL AODs were extracted from the RASCAL estimates. These maps succeed in capturing the spatial gradient of decreasing AOD from Lochiel School to Saturna Island. The temporal sunphotometer plots of Fig. 1 are coherent with these maps in terms of the Lochiel to Saturna gradient of decreasing AOD on 14 and 15 August and more qualitatively in terms of a larger amplitude spatial gradient implying a more rapid temporal variation in the neighborhood of the Lochiel School site. For 14 and 15 August and both stations (4 points) the linear correlation of the AERIAL to CIMEL AODs (1064 nm) was characterized by an R^2 of 0.46 and an rms difference of 0.015. This level of error is acceptable given that the expected AOD error for operational instruments is <0.02 (Eck et al., 1999).

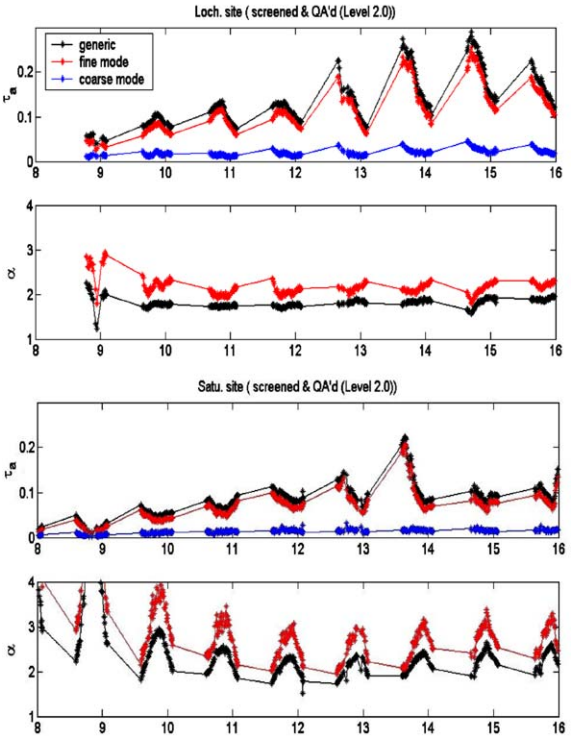

Fig. 1. Variation of the AOD (τ_a) and the Angstrom exponent (α) at 500 nm for the Lochiel School site ("Loch. site") and Saturna Island ("Satu. site"). The black curves represent the total aerosol optical parameter while the red and blue curves represent the fine mode and coarse mode components, respectively. The time axis nomenclature refers to the day in August with the fraction representing the GMT fraction of the day. Local time = GMT − 7 h. Angstrom exponents for Saturna Island are contaminated by interband anomolies induced by small offset problems in the 670 and 1020 nm channels.

4. Active and passive temporal correlations at the Lochiel school site

Consistent with Snyder and Strawbridge's (2004) analysis of turbid air being pushed inland by cleaner sea breeze the fine mode AOD at 500 nm on 13 to 15 August varied from values around 0.2 in the morning to values near 0.1 in the afternoon (Fig. 3a). During this three day period, the diurnal variation of 14 August distinguished itself as a singular optical event in that there was significant fine mode particle sizing change which was not observed or which was weaker on the other days. One sees that the fine mode Angstrom exponent of Fig. 3a rose from about 2–2.5 while the effective radius (r_{eff}) value of the fine mode distribution

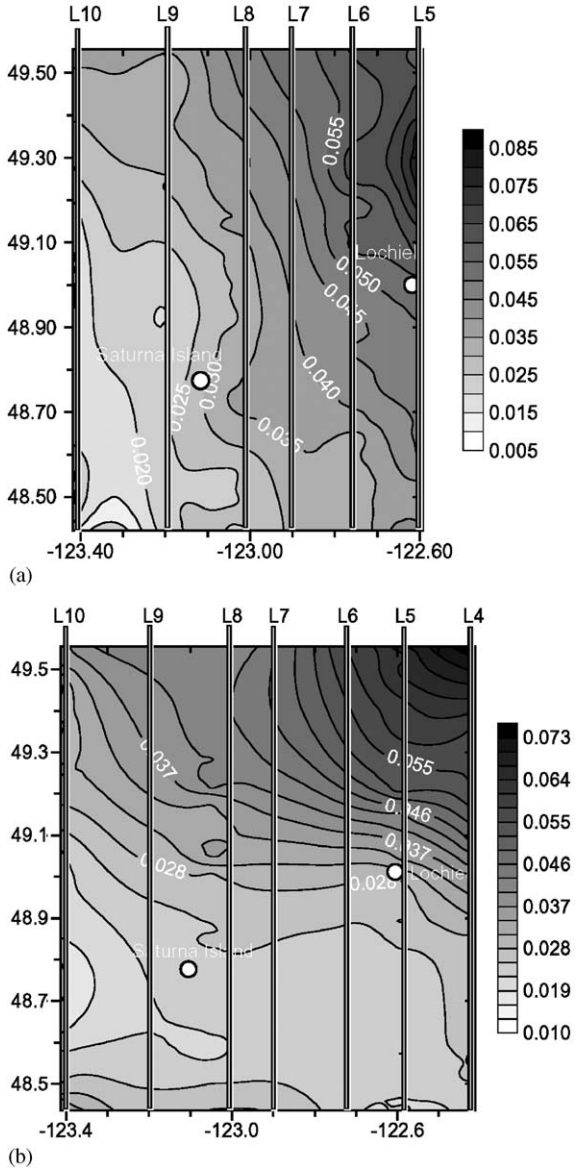

Fig. 2. AOD (1064 nm) contour plots generated by resampling AERIAL AOD transects to a regular grid for (a) 14th August and (b) for 15th August. The approximate flight line positions are indicated along with the flight line labels (L4 etc.). The AERIAL flight times for 14th and 15th August were, respectively, 13:58–15:46 h and 13:52–15:15 h (local daylight savings time). S_a values of 19.0 and 18.3 sr (from the lidar-derived AERIAL S_a values) were employed to generate these AODs on 14th and 15th August, respectively.

(obtained from the Dubovik inversions) decreased from values of about 0.17–0.12 μm. Radiosonde profiles of relative humidity (RH) (Froude, 2003) acquired around 1030 and 1630 PST (roughly 14.7 and 15.0 on the GMT scale of Fig. 3a) showed notably larger RH values in the morning (Table 1). Averages of these profiles over the first 50 mb indicate that 14 August morning period stands out with an average RH well above the afternoon value in terms of optical scattering effects induced by humidification (see for example, Kotchenruther et al., 1999). A similar RH trend was observed on 13 and 15 August but at magnitudes which would be expected to produce significantly smaller optical variations.

The first row of graphs in Fig. 3b show the variation of the sunphotometer AOD at 1064 nm. The colored curves in the second row of graphs show the lidar-derived S_a values while the solid black points show the Dubovik-inversion S_a values (log–log and linear extrapolations were employed, respectively, to transform the AOD and S_a values at 1020–1064 nm for the CIMEL outputs). The error bars in the latter case are a quadrature combination of estimates of the maximum average error in the scattering phase function (Dubovik, 2003) and the maximum error in the single scattering albedo. The error bars in the case of the lidar-derived S_a values correspond to the maximum error of ± 0.02 in the CIMEL AODs (they are only shown for the 306° case to avoid clutter). The large error bars at the end of the day on 14 August and during most of the whole day on 15 August indicate that the error magnitudes were a substantial proportion of the small AODs at 1064 nm. It is also noted that S_a values for elevation angles $<20°$ were excluded form our analysis since it was clear that low signal-to-noise along the line-of-sight were having a significant impact on the computed values. The backscatter ratio profiles in the third row of graphs in Fig. 3b (extracted from the scanning lidar data as described in Strawbridge and Snyder, 2004a) show a distinctly stronger backscatter signal below approximately 800 m in the morning of 14 August. One can also observe that both backscatter profile graphs show significant horizontal stratification, well above the PBL heights reported by Strawbridge and Snyder (2004a); the larger AOD values typically observed in the morning were thus also more vertically dispersed. Strawbridge and Snyder noted that this stratification was related to mountain shear mechanisms affecting pollutant air masses before they are vented out of the LFV by nocturnal land breezes.

The mid-day minimum of lidar-derived S_a values seen in Fig. 3b is likely related to the decrease of the column averaged fine mode particle size (on 14 August in particular) and/or the influence of variations in PBL height as reported by Strawbridge and Snyder (2004a). In the latter case the lower S_a values obtained during the middle of the day on 14 and 15 August correspond to larger PBL heights (~500–900 m) and in general to increased backscatter contributions from the PBL. At 1064 nm the coarse mode particle size contribution has a relatively strong influence on S_a (out of proportion to the small AOD of the coarse mode) and the variable part

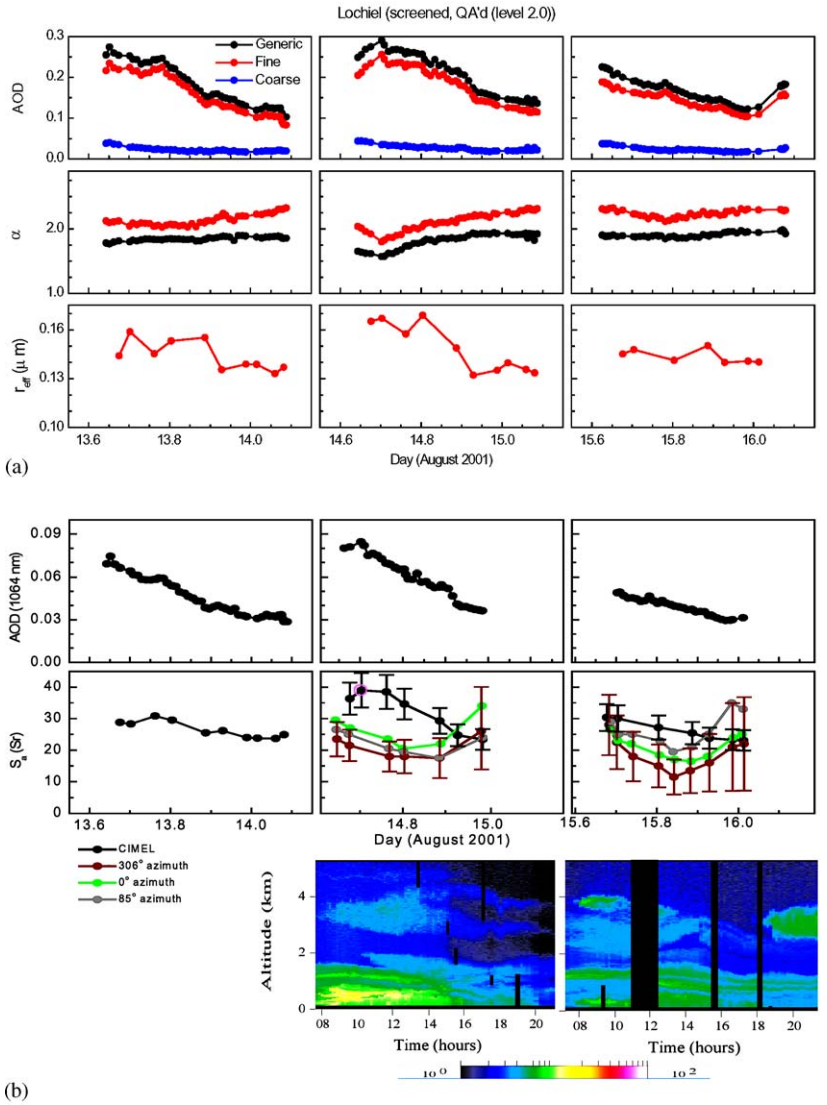

Fig. 3. (a). AOD and Angstrom exponent at 500 nm and effective radius (μm) for 13, 14 and 15 August. Color key is the same as for Fig. 1. (b) AOD and S_a temporal trends and lidar backscatter profiles. The lidar-derived S_a values result from forcing the lidar generated AODs to be equal to the CIMEL AODs. For any of the three RASCAL azimuth directions the lidar profile whose elevation angle was nearest to that of the sun was selected for the AOD and S_a computations. The color enhanced backscatter profiles in the third row of figures are time-height RASCAL composites for 14th and 15th August generated by splicing data from a series of elevation scans at a constant range of 1900 m from the lidar. This produces the equivalent of a zenith-pointing lidar profile every 10 min. Note that there was no lidar data acquired on 13 August.

Table 1
Average RH over the 1st 50 mb (roughly the PBL height as defined in Strawbridge and Snyder (2004a))

Measurements	13 August	14 August	15 August
am	76.7	86.7	74.9
pm	59.2	64.2	56.8

of this influence is largely relegated to the PBL (see Maletto et al. (2003) for example). Because the PBL had a significantly larger optical influence on the integrated lidar returns in the middle of the day it follows that the lower S_a values typical of the coarse mode probably had a greater influence during this time period.

The systematically higher Dubovik-inversion S_a values retrieved on 14 August (Fig. 3b) were suspected, as well, to be related to the optical influence of the coarse mode. We found that these high S_a values could not be explained in terms of departures from nominal retrieval assumptions such as surface albedo values (Yamasoe et al., 1998), non-spherical particles (Dubovik et al., 2000; Mishchenko et al., 1997) or realistic spectral errors in the AOD (the spectral shift error of Dubovik et al. (2000) being somewhat improbable). These retrieved S_a values (and in particular the coarse mode component of S_a) were highly variable and strongly correlated with the retrieved value of m_r (real part of the refractive index).

Angular asymmetries in the local atmosphere were considered as a possibility (since the sunphotometers looked generally south while the lidar scans were constrained to a northern hemisphere) but this could not be quantitatively defended in terms of the comparatively weak (AERIAL-derived) horizontal AOD gradient about the effective optical area surrounding the Lochiel site (which could not be of greater extent than a few kilometers for typical PBL heights).

A closer inspection of the Dubovik inversion results applied to the data of 13, 14 and 15 August indicated that a tenable hypothesis was to simply decouple the coarse mode refractive index from the fine mode refractive index. The inversion algorithm incorporates an assumption of a homogeneous refractive index over the whole size distribution; the impact of this assumption was investigated in Dubovik et al. (2000) but not extrapolated to the effects on S_a. For optical depths not dominated by dust events the coarse mode contribution can only be sensed at scattering angles close to zero and 180°. Since the radiance contribution of the coarse mode is dominated by diffraction (size) effects in the forward direction and is geometrically inaccessible for typical almucanter scans in the backscatter direction, the refractive index influence of the course mode is largely transparent to extinction/sky radiance retrievals. This means that one can manipulate the course mode refractive index (m_c) (and to a lesser extent, the coarse mode size distribution) with very little effect on the inversion residuals (one has no such freedom with the fine mode refractive index, m_f which must remain close to the original inverted value). Fig. 4 shows how S_a, for the case of the worst disparity in Fig. 3b, can be reduced (with only small changes in inversion residuals) by increasing $m_{c,r}$ while maintaining the original Dubovik size distribution and assigning the original retrieved refractive index to the fine mode.

Very little independent data exists in the literature with respect to S_a measurements at wavelengths close to 1064 nm (Anderson et al., 2000). Ackerman's (1998) comparatively high climatologically based values of S_a(1064) for "continental aerosols" were very much influenced by a prescribed coarse mode composed

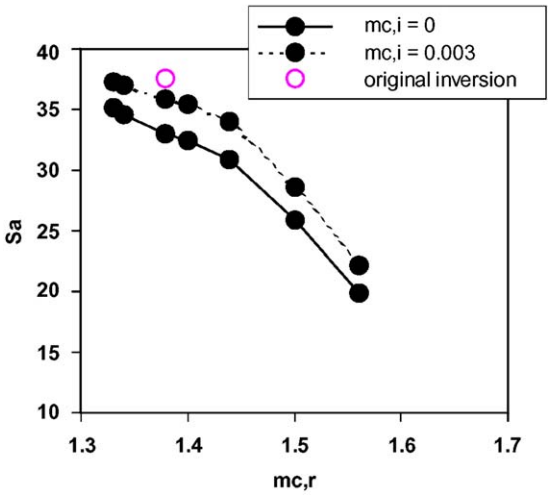

Fig. 4. Decrease of S_a with increasing real part of the refractive index of the coarse mode ($m_{c,r}$). These set of curves, which correspond to excursions from the violet circle value of S_a in Fig. 3b, have very little effect on the Dubovik inversion residuals.

entirely of stongly absorbing (high S_a) dust particles ($m_{c,i} = 0.008$, c.f. Kaufman et al., 2001 for a specific comment on this value and Sokolik and Toon (1999) for some insight as to the reasons for the extreme variability in the computed values of dust $m_{c,i}$). Reagan et al. (2001) reported Dubovik-inversion values of S_a at 1020 nm of ~20 sr in a coarse mode (dust) dominated atmosphere. Ferrare et al. (2001) achieved good agreement between Raman-lidar derived S_a values and Dubovik inversion values but at a wavelength of 355 nm where the fine mode contribution to backscattering is much more dominant.

Surface volume sampling at Langley and in nearby Vancouver indicated that the daytime inorganic coarse mode was largely composed of reacted sea salt in the form of sodium nitrate ($NaNO_3$) as well as some dust and an organic component which was inferred to be $<$~40% by mass (Li, 2003; Dann, 2003). Although such measurements are not necessarily indicative of the column composition they do suggest the possibility of a strongly scattering/weakly absorbing coarse mode refractive index (high $m_{c,r}$ and low $m_{c,i}$). A coarse mode refractive index dominated by soluble $NaNO_3$ (the dry value being 1.58 – 0i at 1.0 μm as per Palik (1998) and $m_r = 1.58$ at some visible wavelength as per Tang (1996) and soluble organics (dry value of 1.53 − 0i at 0.55 μm as per Ebert et al., 2002) is enough of a difference, relative to the refractive index which yielded the violet case study point of Figs. 3b and 4 (1.38 − .005i), to induce a significant decrease in the CIMEL value of S_a. Note that the symbolic "0i" associated with the complex

part of these refractive indices is meant to imply that there is no measurable absorption influence (inferred from the references given).

The AOD is a function of both particle number and size; the available optical and meteorological evidence suggests that the AOD decrease of 14 August was induced not only by changing number densities of fine mode polluting particles but as well by significant decreases in the fine mode particle size associated with RH particle sizing effects (in point of fact the relatively rapid increase of the fine mode Angstrom exponent in Fig. 3a versus a relatively small decrease in AOD implies that the particle size change contribution must be dominant; c.f. Fig. 1 of O'Neill et al., 2002). Unambiguous RH optical effects are not uncommon in point volume measurements (see for example, Kotchenruther et al., 1999) but are more difficult to verify for small amplitude measurements of vertically integrated AOD (the data in the ground breaking AOD apportionment studies of Hegg et al. (1997) show virtually no relationship for AODs <0.2). The fact that the indicators in Fig. 3a and the RH values of Table 1 do not show or only weakly imply a similar decreasing particle size trend for 13 and 15 August confirms that the typical diurnal decrease of the stagnant period was strongly influenced by the simple removal of polluting particles.

5. Summary and conclusions

Sunphotometry and sky radiometry data at the Lochiel School site and Saturna Island sunphotometer sites were acquired synchronously with ground-based scanning lidar (RASCAL) and airborne lidar (AERIAL) data during the Pacific 2001 Air Quality Study. The passive and active data were analyzed along with meteorological and microphysical data in order to better understand their degree of spatio-temporal inter-consistancy during the stagnant period of 13 to 16 August, 2001. A mid-day minimum in lidar-derived S_a values, was attributed, at least in part, to the RH induced optical influence of the column integrated fine mode and/or to the optical influence of coarse mode particles in the PBL. A systematic overestimate of Dubovik-inversion S_a values relative to lidar-derived S_a values was hypothesized to be due to a course mode refractive index which was substantially different from the refractive index returned by the Dubovik algorithm. AOD differences at 1064 nm were within maximum error bounds of 0.02 and the (4 point) correlation was significant when comparing the sunphotometry at the Lochiel site and Saturna Island with spatial maps generated from AERIAL. Daily temporal trends of optical and microphysical parameters derived using sunphotometer and sky radiance data at this site were largely consistent with information deduced from the lidar and meteorological data. While the daily AOD decrease was clearly associated with particle removal induced by daytime sea-breeze advection, a significant part of this decrease was associated with decreasing RH growth effects on at least one day.

The combination of ground-based scanning lidar, airborne mapping lidar and multi-station sun and sky radiometry promotes a more comprehensive appreciation of local and regional aerosol optical behavior and, along with meteorological and microphysical measurements, lends confidence to mechanistic analyses of complex pollution events. The passive/active comparisons presented in this communication are continuing with an array of data sets acquired during different conditions of local and regional turbidity. In particular the angular information contained in the lidar elevation scans is being fully exploited to extract S_a using relative line-of-sight relationships (see Spinhirne et al. (1980) for example). This technique yields an essentially independent measure of S_a which we are currently evaluating.

Acknowledgements

This work was partially supported by the Canadian Foundation for Climate and Atmospheric Sciences, Environment Canada, the National Sciences and Engineering Research Council, and the AERONET group of NASA. The authors would also like to thank Michael Harwood, and Michael Travis (Meteorological Service of Canada), Mark Barton and Roxanne Vingarzan (Pacific Yukon Region, Environment Canada), Gerri Crooks (site technician at Saturna Island) and Patrick Cliche (CARTEL) for their attentive technical support during the Pacific 2001 experiment.

References

Ackerman, J., 1998. The extinction-to-backscatter ratio of tropospheric aerosol: a numerical study, vol. 15, pp. 1043–1050.

Anderson, T.L., Masonis, SJ., Covert, D.S., Charlson, R.J., Rood, M.J., 2000. In situ measurement of aerosol extinction-to-backscatter ratio at a polluted continental site. Journal of Geophysical Research 105, 20907–20915.

Ansmann, A., Wagner, F., Muller, D., Althausen, D., Herber, A., von Hoyningen-Huene, W., Wandinger, U., 2002. European pollution outbreaks during ACE 2: optical particle properties inferred from multiwavelength lidar and star-Sun photometry. Journal of Geophysical Research 107, doi:10.1029/2001JD001109.

Dann, T., 2003. Personal communication.

Dubovik, O., 2003. Personal communication.

Dubovik, O., King, M.D., 2000. A flexible inversion algorithm for retrieval of aerosol optical properties from Sun and sky

radiance measurements. Journal of Geophysical Research 105, 20673–20696.

Dubovik, O., Smirnov, A., Holben, B.N., King, M.D., Kaufman, Y.J., Eck, T.F., Slutsker, I., 2000. Accuracy assessments of aerosol optical properties retrieved from AERONET Sun and sky-radiance measurements. Journal of Geophysical Research 105, 9791–9806.

Ebert, M., Weinbruch, S., Rausch, A., Gorzawski, G., Helas, G., Hoffmann, P., Wex, H., 2002. Complex refractive index of aerosols during LACE 98 as derived from the analysis of individual particles. Journal of Geophysical Research 107 (D21), LAC3-1–LAC3.

Eck, T.F., Holben, B.N., Reid, J.S., Dubovik, O., Smirnov, A., O'Neill, N.T., Slutsker, I., Kinne, S., 1999. The wavelength dependence of the optical depth of biomass burning, urban and desert dust aerosols. Journal of Geophysical Research 104, 31,333–31,350.

Ferrare, R., Ismail, S., Browell, E., Brackett, E., Clayton, M., Kooi, S., Melfi, S.H., Whiteman, D., Schwemmer, G., Evans, K., Russell, P., Livingston, J., Schmid, B., Holben, B., Remer, L., Smirnov, A., Hobbs, P.V., 2000. Comparison of aerosol optical properties and water vapour among ground and airborne lidars and sun photometers during TARFOX. Journal of Geophysical Research 105, 9917–9933.

Ferrare, R., Turner, D.D., Heilmann Brasseur, L., Feltz, W.F., Dubovik, O., Tooman, T.P., 2001. Raman measurements of the aerosol extinction-to-backscatter ratio over the Southern Great Plains. Journal of Geophysical Research 106 (D17), 20333–20347.

Froude, F., 2003. Personal communication.

Hegg, D.A., Livingston, J., Hobbs, P.V., Novakov, T., Russel, P., 1997. Chemical apportionment of aerosol column optical depth off the mid-Atlantic coast of the United States. Journal of Geophysical Research 102, 25293–25303.

Holben, B.N., et al., 1998. AERONET—A federated instrument network and data archive for aerosol characterization. Remote sensing of the Environment 66, 1–16.

Kaufman, Y.J., Tanré, D., Dubovik, O., Karnieli, A., Remer, L.A., 2001. Absorption of sunlight by dust as inferred from satellite and ground-based remote sensing. Geophysical Research Letters 28 (8), 1479–1482.

Kotchenruther, R.A., Hobbs, P.V., Hegg, D.A., 1999. Humidification factors for atmospheric aerosols off the mid-atlantic coast of the United States. Journal of Geophysical Research 104, 2239–2251.

Li, S.-M., 2003. Personal communication.

Li, S.-M., 2004. A concerted effort to understand the ambient particulate matter in the Lower Fraser Valley: the Pacific 2001 air quality study. Atmospheric Environment, this issue, doi:10.1016/j.atmosenv.2004.04.038.

Maletto, A., McKendry, I.G., Strawbridge, K.B., 2003. Profiles of particulate matter size distributions using a balloon-borne lightweight aerosol spectrometer in the planetary boundary layer. Atmospheric Environment 37, 661–670.

Mishchenko, M.I., Travis, L.D., Kahn, R.A., West, R.A., 1997. Modelling phase functions for dustlike tropospheric aerosols using a shape mixture of randomly oriented polydispersive spheroids. Journal of Geophysical Research 102 (No. 14), 16831–16847.

O'Neill, N.T., Eck, T.F., Holben, B.N., Smirnov, A. Royer, A., Li, Z., 2002. Optical properties of Boreal forest fire smoke derived from sunphotometry. Journal of Geophysical Research 107, doi:10.1029/2001JD000877.

O'Neill, N.T., Eck, T.F., Smirnov, A., Holben, B.N., Thulasiraman, S., 2003. Spectral discrimination of coarse and fine mode optical depth. Journal of Geophysical Research 108, (D17), 4559-4573, 10.1029/2002JD002975.

Palik, E.D., 1998. Handbook of optical constants of solids, vol. III. Academic Press, Toronto.

Pelon, J., Flamant, C., Chazette, P., Leon, J.-F., Tanre, D., Sicard, M., Satheesh, S.K., 2002. Characterization of aerosol spatial distribution and optical properties over the Indian Ocean from airborne LIDAR and radiometry during INDOEX'99. Journal of Geophysical Research 107, 8029.

Reagan, J.A., Thome, K.J., Powell, D.M., 2001. Towards Establishing an aerosol extinction-to-backscatter ratio climatology. Proceedings of A&WMA Specialty Conference on Regional Haze and Global Radiation Balance—Aerosol Measurements and Models, 2–5 October Bend, OR, 11 pp.

Smirnov, A., Holben, B.N., Eck, T.F., Dubovik, O., Slutsker, I., 2000. Cloud screening and quality control algorithms for the AERONET data base. Remote Sensing of Environment 73, 337–349.

Snyder, B.J., Strawbridge, K.B., 2004. Meteorological summary of the Pacific 2001 air quality field study. Atmospheric Environment, this issue, doi:10.1016/j.atmosenv.2004.02.068.

Sokolik, I.N., Toon, O.B., 1999. Incorporation of mineralogical composition into models of the radiative properties of mineral aerosol from UV to IR wavelengths. Journal of Geophysics 104 (D8), 9423–9444.

Spinhirne, J.D., Reagan, J.A., Herman, B.M., 1980. Vertical distribution of aerosol extinction cross section and inference of aerosol imaginary index in the troposphere by lidar technique. Journal of applied Meteorology 19, 426–438.

Strawbridge, K.B., Snyder, B.J., 2004a. Planetary boundary layer height determination during Pacific 2001 using the advantage of a scanning lidar instrument. Atmospheric Environment, this issue, doi:10.1016/j.atmosenv.2003.10.065.

Strawbridge, K.B., Snyder, B.J., 2004b. Daytime and nighttime aircraft lidar measurements showing evidence of particulate matter transport into the northeastern valleys of the Lower Fraser Valley, B.C. Atmospheric Environment, this issue, doi:10.1016/j.atmosenv.2003.10.036.

Tang, I.N., 1996. Chemical and size effects of hygroscopic aerosols on light scattering coefficients. Journal of Geophysics 101 (D14), 19245–19250.

Yamasoe, M.A., Kaufman, Y.J., Dubovik, O., Remer, L.A., Holben, B.N., Artaxo, P., 1998. Retrieval of the real part of the refractive index of smoke particles from Sun/sky measurements during SCAR-B. Journal of Geophysics 103 (D24), 31,893–31,902.